科学通报 2023 年 第 68 卷 第 12 期: 1443 ~ 1458
水循环的地质演变专辑 评 述
《中国科学》杂志社 SCIENCE CHINA PRESS

轨道驱动对高低纬水循环的影响特征: 海冰和降水

吴志鹏[1,2,3], 尹秋珍[2*], 梁明强[2], 郭正堂[1,3,4], 史锋[1,4], 陆浩[1], 苏倩倩[2], 吕安琪[2]

1. 中国科学院地质与地球物理研究所, 中国科学院新生代地质与环境重点实验室, 北京 100029;
2. Georges Lemaître Center for Earth and Climate Research, Earth and Life Institute, Université catholique de Louvain, Louvain-la-Neuve 1348, Belgium;
3. 中国科学院大学地球与行星科学学院, 北京 100049;
4. 中国科学院生物演化与环境卓越创新中心, 北京 100044
* 联系人, E-mail: qiuzhen.yin@uclouvain.be

2022-08-08 收稿, 2022-09-26 修回, 2022-09-28 接受, 2022-11-16 网络版发表
国家自然科学基金(41888101)资助

摘要 轨道尺度上的水循环及其对轨道三要素、温室气体和冰盖的响应一直是古气候学界研究的热点科学问题之一. 海冰和降水作为水循环的两个重要组成部分, 其变化更是备受关注. 研究海冰和降水在轨道尺度上的变化, 特别是对外部驱动的响应机理、内部过程和反馈机制, 有望对现代海冰和降水变化的理解及其未来趋势预测提供长尺度的背景参考. 最新研究结果表明, 在轨道尺度上北半球海冰对太阳辐射的变化更敏感, 而南半球海冰对温室气体的变化更敏感. 就轨道三要素而言, 北半球海冰主要受岁差控制, 而南半球海冰主要受斜率控制. 岁差、斜率和CO_2在全球不同区域降水中的相对重要性随时间和空间不同而发生变化. 受赤道最大太阳辐射影响, 热带降水中还含有明显的半岁差信号. 此外, 缓慢的轨道尺度太阳辐射变化可以通过影响北极海冰变化来引起大西洋经向翻转环流(Atlantic meridional overturning circulation, AMOC)百年-千年尺度的突变, 从而引起全球温度和降水随之发生改变. 在东亚季风区, 中国南方夏季降水受冰盖影响显著, 冰盖主要通过影响热带辐合带(inter-tropical convergence zone, ITCZ)的季节性摆动来影响降水; 而中国北方夏季降水主要受太阳辐射控制, 以岁差信号占主导; 太阳辐射和冰量对夏季风降水的影响具有较强的区域性和非线性特征.

关键词 水循环, 降水, 海冰, 轨道驱动, 冰盖, 高低纬相互作用

水循环对维持全球气候-环境系统的稳定性发挥着至关重要的作用, 同时也是地球能够成为我们“绿色宜居家园”的关键因素之一[1,2]. 水循环还影响着碳循环, 这进一步突出了水循环在全球气候-环境-生态中的作用[3,4]. 因此, 对全球水循环开展深入研究不仅可以加强对气候-环境相互作用的理解, 还有望为实现我国碳达峰、碳中和“双碳”目标提供理论参考.

就地球表层系统的水循环而言, 高纬冰冻圈系统和低纬季风系统的作用至关重要, 且二者通过海洋和大气环流紧密地联系在一起, 共同控制着全球水循环[5~9]. 要深入理解全球水循环, 加强对现代全球水循环的研究毋庸置疑十分重要, 而探讨水循环的地质演变也是其中不可或缺且尤为重要的一部分. 水循环的地质演变是从更长时间尺度探讨全球水循环, 有助于更好地理解水循环对外部驱动的响应机理及其相关的内部过程和反馈机制[6~10]. 加强对水循环的地质演变的研究还能够为更好地理解当前全球水循环及其对未来趋势的预测提供重要的参考.

引用格式: 吴志鹏, 尹秋珍, 梁明强, 等. 轨道驱动对高低纬水循环的影响特征: 海冰和降水. 科学通报, 2023, 68: 1443–1458
Wu Z P, Yin Q Z, Liang M Q, et al. The effect of astronomical forcing on water cycle: Sea ice and precipitation (in Chinese). Chin Sci Bull, 2023, 68: 1443–1458, doi: 10.1360/TB-2022-0833

另一方面，地球轨道周期信号不仅广泛存在于第四纪[3,11~16]，甚至在新生代乃至更久远的地质历史时期的记录中均有发现[10,17,18]. 已有的研究表明，轨道尺度的外部驱动不仅能够解释数万年至数十万年尺度的气候变化[19~22]，还能够解释不少亚轨道尺度和构造尺度的气候现象[17,18,23~27]. 因此，加强对轨道尺度气候变化的研究不仅能够加深对气候变化机理、过程的认识，还有望打破气候变化研究在不同时间尺度上的束缚，将不同时间尺度的气候变化较为有效地联系起来.

就水循环的地质演变而言，轨道尺度的水循环无疑是一个重点研究内容，其将会是全面理解全球水循环的重要窗口. 海冰和降水作为水循环的两个重要组成部分，长期以来一直备受科学界的关注[21,28]. 海冰和降水轨道尺度上的变化不仅受到外部驱动(如太阳辐射、CO_2和冰盖)的控制，而且受到内部反馈(如植被反馈)的影响[19~21,29,30]. 为了更好地理解海冰和降水轨道尺度上的变化，本文围绕南北半球海冰和全球降水(特别是季风降水)对不同外部驱动的响应、热带降水中的半岁差信号和太阳辐射引起的降水突变等科学问题，简要综述前人利用地质记录和数值模拟等方法取得的认识，并较为详细地介绍本团队近些年在这些方面取得的进展，最后提出一些当前研究所面临的不足以及未来研究亟须加强的方向.

1 南北半球海冰的轨道尺度变化

海冰是冰冻圈系统的重要组成部分之一，由于其高反射率决定的反射率-温度的反馈作用和低热导率决定的隔热效果，对高纬和全球的气候系统发挥着极为重要的作用[28]. 海冰的形成与融化不仅改变了海洋对太阳辐射的吸收、海洋和大气之间的能量交换，还影响了海洋的盐度结构，进而影响了全球的海洋、大气环流[31]. 另外，海冰的变化还影响了全球海平面的变化、冰盖的物质平衡以及高纬的生态系统和生物-地球化学循环[32~34].

目前，利用多指标地质记录重建和数值模拟等方法，对轨道尺度上海冰变化的研究已取得了很大的进展. 重建过去海冰变化的方法主要有: 浮游有孔虫[35]、底栖有孔虫[36]、浮游与底栖有孔虫的比例[37]、甲藻[38]、颗石藻[39]、海冰碎屑沉积物[40]和有机生物标志物IP25[41]等. 格陵兰海冰重建结果表明，相比于早全新世，晚全新世海冰相对较少[42]. 楚科奇海海冰重建结果也表明，海冰自过去9000年以来显著下降[38]. 但加拿大东部海冰重建结果却显示，早全新世处于季节性无冰的状态[43]. 末次冰期以来，鄂霍次克海海冰变化以岁差信号为主，主要受控于北半球高纬太阳辐射[44]. 末次间冰期，由于北半球高纬较高的夏季太阳辐射，北半球大部分地区呈现夏季无冰的状态[45]. 末次间冰期之前，北极海冰的记录相对较少，且分辨率相对较低. 少量分辨率相对较高且持续时间相对较长的海冰记录显示，北极海冰在深海氧同位素阶段11(MIS-11)由季节性海冰向多年生海冰发生转变，且北极海冰变化显示了明显的岁差和斜率信号，并以岁差信号占主导[46~48]. 相对于北极海冰，南大洋海冰的地质记录更少. 其中重建时间较长、分辨率相对较高且沉积连续的南极冰芯Dome C中钠盐的重建结果表明，间冰期南大洋海冰在MIS-13范围最大，而在MIS-5范围最小[15]. 此外，过去80万年南大洋海冰的变化以10万年的冰期-间冰期旋回信号占主导，也包含相对较弱的岁差和斜率信号[15]. 总体而言，地质记录重建的结果表明，北极和南大洋海冰在轨道尺度上显示出不同的演变特征: 北极海冰以岁差信号占主导，主要受控于太阳辐射; 而南大洋海冰以10万年的信号占主导，主要表现为冰期-间冰期旋回变化.

除地质记录外，数值模拟也被广泛用于探讨北极和南大洋海冰的变化及其对不同外部驱动因素的响应. 不同时期(中全新世、末次冰盛期和末次间冰期)的敏感性实验结果表明，数值模拟能够较好地模拟出北极和南大洋海冰的变化，但不同模型之间也存在着显著性差异. 相对于工业革命前，由于中全新世更高的北半球高纬夏季太阳辐射，所有的模拟结果都显示出较少的北极夏季海冰[49]. 同时部分模拟结果也显示中全新世北极冬季海冰减少，这主要是由于海洋的记忆功能，将夏季的能量部分储存起来，然后在冬季释放出来; 然而，也有部分模拟结果显示中全新世冬季海冰增多，主要是直接响应更低的冬季太阳辐射[31]. 而对于中全新世南大洋海冰，不同模型的模拟结果差异性相对较大，难以得到相对一致的结论[31,50]. 末次冰盛期，几乎所有的模拟结果都显示北极和南大洋夏季、冬季海冰均增多，但不同模型模拟的北极和南大洋海冰的增加幅度差异却很大，最大差异超过6倍[51]. 末次间冰期，由于北半球高纬更高的夏季太阳辐射，大多数模型模拟结果显示较少的北极海冰，甚至部分模型模拟结果显示北半球在此时期可能处于夏季无冰的状态. 这与钻孔PS2200-5、PS51/038-3、S2757-8和PS2138-2生物标志化合物重建的北冰洋海冰具有很好的一致性[52~55]. 此

外，瞬变模拟结果显示，当CO_2在一定范围(190~260 ppmv，1 ppm=10^{-6} L/L)之内时，北极海冰主要受控于太阳辐射，并以岁差信号占主导，这与鄂霍次克海海冰重建较为一致[44]. 相比之下，南大洋海冰的变化以10万年的信号为主，斜率的信号相对较强，这与南极冰芯重建的南大洋海冰结果具有很好的一致性[56].

关于南北半球海冰对太阳辐射和CO_2的差异性响应，最近的数值模拟结果也取得了一些新的进展(图1). 利用因子分离技术分别研究太阳辐射和CO_2对过去9个间冰期海冰的影响，结果发现北极年均海冰的变化主要受控于太阳辐射，而CO_2对南大洋年均海冰变化的作用更显著[20,57]. 进一步分析海冰的季节性变化发现，北极海冰夏季变化较大，且主要受控于北半球高纬夏季太阳辐射. 相对于北极海冰，南大洋海冰的季节性变化差异相对较小，而南大洋冬季海冰的变化主要受控于CO_2，夏季海冰的变化同时受控于太阳辐射和CO_2[20,57]. 因此，对南大洋年均海冰变化而言，CO_2的作用更显著. 在太阳辐射和CO_2共同影响下，过去9个间冰期北极夏季海冰相比现在和未来均较少，这主要是因为过去9个间冰期较高的北半球夏季太阳辐射；而相比于未来，过去9个间冰期年均和季节性南大洋海冰均较多，这主要是因为过去9个间冰期较低的CO_2[20]. 就轨道三要素而言，太阳辐射单因子驱动下长达9万多年的瞬变模拟结果显示，北极海冰主要受岁差控制，较小的岁差对应较少的海冰，较大的岁差对应较多的海冰；而南大洋海冰主要受斜率控制，高斜率对应较少的海冰，低斜率对应较多的海冰[19]. 不同的驱动机制导致北极和南大洋海冰对斜率和岁差的差异性响应. 北极海冰主要受控于以岁差信号占主导的北半球高纬夏季太阳辐射；而南大洋海冰对以斜率信号为主的年均太阳辐射和南半球西风响应更敏感[19]. 总体而言，北极海冰主要受太阳辐射和岁差的控制，这与北冰洋长时间尺度、高分辨率的海冰记录具有很好的一致性[46~48]；而南大洋海冰主要受CO_2和斜率的控制.

这种南北半球海冰受轨道驱动的不一致性变化，其根本原因主要是北冰洋和南大洋所处的地理位置不同. 北冰洋是一个相对封闭的海盆，深度较浅，且大部分位于北极圈以内的极高纬地区，导致该地区冬季接受到的太阳辐射很少，主要受以岁差占主导的夏季太阳辐射的影响[19,20,57]. 在北冰洋，夏季太阳辐射不仅影响夏季海冰，而且通过海冰和海洋的反馈机制，对冬季海冰和海表温的影响更大，这种现象被称为夏季太阳辐射的残留效应(summer remnant effect)[57]. 另一方面，北冰洋被陆地包围，陆地上的植被对海冰也有影响，而植被变化也主要受岁差控制[57]. 相比北冰洋，南大洋位于纬度较低、深度较深且开放的海洋中，这些特征使得它对全球性以及全年性的驱动力更为敏感[19,20,57]，如温室气体. 而一个给定纬度的全年总的太阳辐射和半球总的太阳辐射完全受控于斜率[58]，使得南大洋海冰对斜率也较为敏感. 为了更好地探讨南北半球海冰对太阳辐射、CO_2和冰盖的差异性响应及其地质记录与数值模拟的对比，一方面，需要加强高分辨率、长时间尺度南北半球海冰记录的重建；另一方面，需要利用不同模型开展太阳辐射和CO_2共同驱动，以及太阳辐射、CO_2和冰盖全驱动的长时间尺度瞬变模拟实验.

2 全球降水的轨道尺度变化

轨道尺度上全球降水变化不仅受到外部驱动(太阳辐射、CO_2和冰盖)的影响，还受到内部过程和反馈作用的调控. 此外，轨道驱动还能引发一些亚轨道尺度的降水变化，例如半岁差信号和降水突变事件. 下面主要探讨降水对岁差、斜率、CO_2和冰盖的区域差异性响应以及降水中的半岁差信号和突变信号.

2.1 区域性降水对岁差、斜率、CO_2和冰盖的差异性响应

全球降水变化对全球水循环发挥着直接的控制作用. 相对于温度，降水的区域差异性更强[60]. 轨道尺度上，降水对岁差、斜率、CO_2和冰盖的区域差异性响应一直是古气候学界研究的重点科学问题之一.

地质记录重建结果表明，不同区域降水对岁差、斜率、CO_2和冰盖的响应存在着显著的差异. 例如，格陵兰岛东北部石笋记录表明，由于受北半球高纬夏季太阳辐射的影响，当地的降水在MIS-15相比于工业革命前更多[61]. 贝加尔湖孢粉的记录结果显示，冰盖对末次间冰期和全新世期间的当地年均降水变化具有重要影响[62]. 而中纬度降水的集成记录显示，全新世南北半球中纬度降水均主要受控于高低纬太阳辐射梯度差[63,64]. 日本海孢粉记录重建的东亚夏季风降水[65]和的的喀喀湖沉积物重建的南美季风降水[66]均显示其主要受控于太阳辐射，以岁差信号占主导. 而位于核心季风区外的巴西热带东部沿海地区的海洋沉积物记录显示，过去85万年该地降水主要受控于两半球夏季太阳辐射梯度差，以斜率信号占主导[67]. 伊比利亚孢粉记录

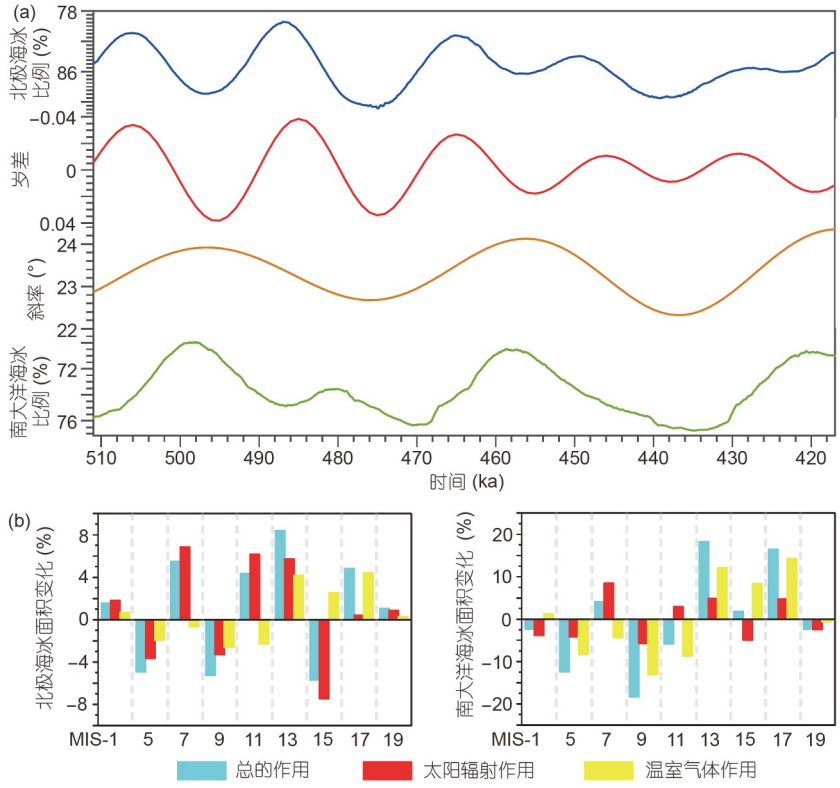

图 1 北极和南大洋海冰变化[19,20]. (a) 轨道驱动下LOVECLIM模拟的北极和南大洋年均海冰变化[19]及其与岁差和斜率[59]的对比. 从上到下依次为: 北极海冰比例、岁差、斜率、南大洋海冰比例. (b) 太阳辐射和温室气体对过去80万年每个间冰期北极和南大洋年均海冰变化单独和总的作用. 海冰面积变化(%)是与参考实验相比较[20]

Figure 1 The variations of the Arctic and Southern Ocean sea ice[19,20]. (a) LOVECLIM-simulated annual mean Arctic and Southern Ocean sea ice variations under the orbital forcing[19] and their comparison with precession and obliquity[59]. From top to bottom: Arctic sea ice fraction, climatic precession, obliquity, and Southern Ocean sea ice fraction. (b) Individual and combined effects of insolation and greenhouse gases (GHG) on the annual mean Arctic and Southern Ocean sea ice at each interglacial over the past 800 ka. The anomalies (%) are deviations from the reference experiment[20]

显示当地冬季降水主要受控于太阳辐射, CO_2的作用相对很小[68]. 此外, 大量的地质记录显示, 地中海降水主要受控于太阳辐射, 以岁差信号占主导[69~71]. 而新西兰北岛凯伊维湖沉积物显示, CO_2对当地末次冰期降水影响较大[72].

除地质记录外, 数值模拟也被广泛用于探讨降水的区域差异性响应. 例如, HadCM3敏感性实验结果显示, 格陵兰岛降水主要受控于北半球高纬夏季太阳辐射, 这与当地石笋记录重建的降水具有很好的一致性[61]. LOVECLIM瞬变实验结果表明, 伊比利亚和地中海降水均主要受控于太阳辐射, 以岁差信号占主导, 这也与利用孢粉等地质记录重建的当地降水具有很好的一致性[68,70]. 最近, 利用数值模拟的方法对不同区域降水的差异性研究也取得了一些新的认识. HadCM3和气候模拟器的结果显示, 过去260万年东亚夏季降水和年均降水具有很强的区域性和时期差异[30]. 中国北方, 夏季降水在整个第四纪均主要受控于太阳辐射, 以岁差信号为主; 年均降水在早更新世主要受控于太阳辐射, 以岁差信号为主, 而在中晚更新世同时受控于太阳辐射和冰盖. 中国南方, 夏季降水在早更新世以2万年和4万年的信号为主, 在中晚更新世则以4万年和10万年的信号为主; 而年均降水在早更新世以4万年的信号为主, 中晚更新世则以10万年的信号为主. 这一结果与东亚季风区不同类型记录所反映的降水变化具有很好的一致性[30].

此外, 利用LOVECLIM1.3对MIS-11和MIS-13两个间冰期进行的瞬变模拟结果表明, 岁差、斜率和CO_2在全球不同区域降水中的相对重要性随地区和时间而变化(图2)[73]. 具体表现为: 在高纬度, 降水与斜率和负岁差呈现正相关关系, 当斜率越大、岁差越小, 夏季太阳辐射越强, 降水增多, 这与HadCM3敏感性实验结果和格陵兰岛石笋记录所反映的降水变化较为一致[61]. 中

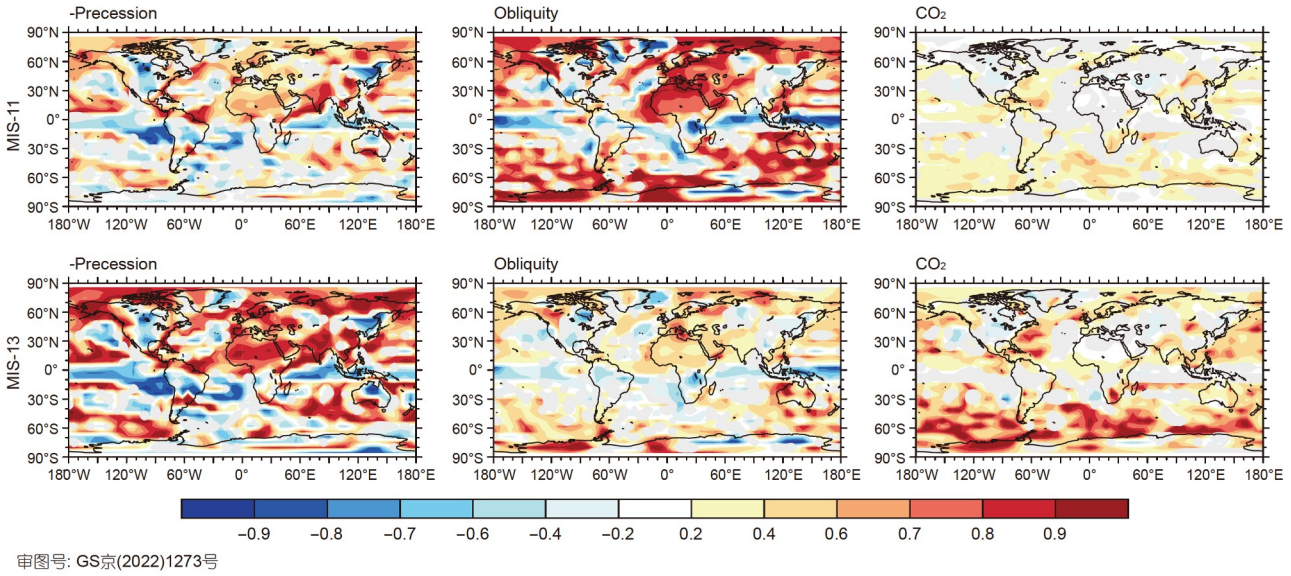

图 2 LOVECLIM模拟的MIS-11和MIS-13时期全球年降水与负岁差、斜率和CO_2的多元线性回归图[73]. 灰色阴影区域代表相关系数在统计意义上不显著(P>0.05). 当岁差越小时, 北半球夏季太阳辐射越高; 而岁差越大时, 北半球夏季太阳辐射越低. 为了从太阳辐射的角度来探讨降水和岁差的关系, 本文用负岁差来进行多元线性回归分析

Figure 2 Coefficients of multi-linear regressions between LOVECLIM-simulated annual mean precipitation and -precession, obliquity and CO_2 during MIS-11 and MIS-13[73]. Regions where the respective coefficient is not statistically significant (P>0.05) are grey shaded. Precession minimum (maximum) corresponds to high (low) summer insolation in the Northern Hemisphere. In order to study the relationship between precession and precipitation from the perspective of insolation, the inverse value of precession is used in the regression analysis

纬度温带北美地区, 降水与负岁差呈现负相关关系[73], 这与CCM3.10模拟的降水变化[74]和数据集成的结果具有很好的一致性[75,76], 均显示当夏季太阳辐射高时, 降水减少. 在北非、印度和东亚季风区, 降水与负岁差呈现正相关关系; 而南半球季风区, 降水与负岁差呈现负相关关系. 这主要是因为低纬度季风降水变化主要受控于低纬夏季太阳辐射, 这与石笋记录所反映的降水变化高度吻合[77,78]. 相对于全球其他地区, CO_2对南半球中高纬度的影响相对较大[73]. 就MIS-11和MIS-13两个间冰期而言, 岁差和CO_2的影响在MIS-13相对更强, 而斜率的影响在MIS-11相对更强(图2), 这主要是因为岁差和CO_2的振幅变化在MIS-13相对更大, 而斜率的振幅变化在MIS-11相对更大[73]. 区域性降水一直以来是模拟中的一个难题, 但是上述提到的地质记录和模拟结果都表明, 不同区域和不同时间段的降水对岁差、斜率、CO_2和冰盖的响应存在显著差异, 因此针对特定地区和特定时间段的详细研究显得尤为重要.

2.2 热带降水中的半岁差信号

在近几十年的古气候研究中, 半岁差信号获得了越来越广泛的关注. 这主要是因为在众多的亚轨道尺度气候变化中, 半岁差信号能直接用赤道最大太阳辐射的线性驱动来解释[79]. 此外, 半岁差信号对全面理解第四纪其他重大气候变化事件具有重要意义, 其中包括Dansgaard-Oeschger(DO)事件[80]和中更新世革命[79,81]等. 目前, 半岁差信号已被发现在不同类型的地质记录中, 其中包括海洋沉积物[82,83]、植被[84]、湖相沉积物[85]、黄土[86]和冰芯[3]等. 就反映降水的气候指标而言, 半岁差信号也被报道[85,87~89]. 但是, 关于半岁差信号的驱动机制目前还存在较大的争议, 主要有以下4种观点: (1) 赤道最大太阳辐射[79]; (2) 南北半球相互作用[3,81]; (3) 气候系统对岁差驱动的内部反馈[90]; (4) 气候系统的非线性相互作用[3].

最新模拟结果显示, 受赤道最大太阳辐射影响, 热带降水中也有明显的半岁差信号(图3)[19], 这与地质记录重建的赤道东非[85,87]、赤道太平洋[88]和埃塞俄比亚南部[89]降水中的半岁差信号具有很好的一致性. 对MIS-11、MIS-13和MIS-19三个间冰期热带降水中的半岁差信号进一步分析发现, 半岁差信号的强弱受岁差和斜率振幅变化的影响. 当偏心率越大时, 岁差的振幅变化越大, 半岁差信号越强; 当偏心率越小时, 岁差的振幅变化越小, 半岁差信号越弱. 而斜率对半岁差信号

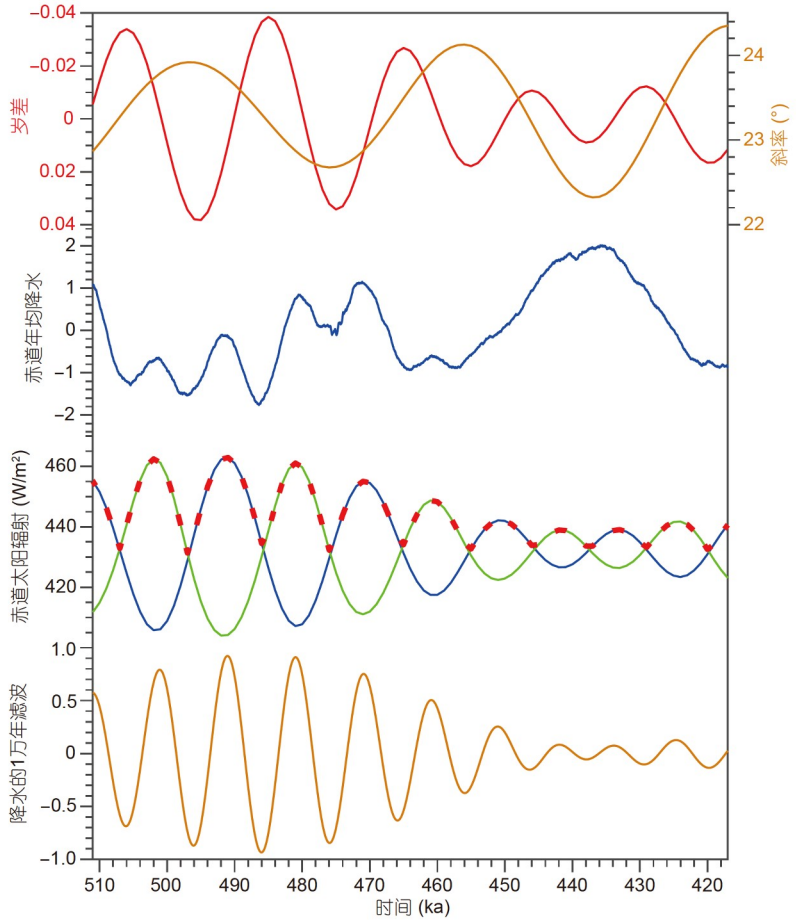

图 3 LOVECLIM模拟的热带降水中的半岁差信号及其驱动机制[19]. 从上到下依次为: 岁差(红线)和斜率(橙线)[59]; 赤道年均降水(标准化); 赤道最大太阳辐射: 蓝线为3月日照量, 绿线为9月日照量, 红色虚线为两者最大值[59]; 赤道年均降水中的半岁差信号

Figure 3 The LOVECLIM-simulated half-precession signal in the tropical precipitation and its forcing mechanism[19]. From top to bottom: Preceesion (red line) and obliquity (orange line)[59]; standardized annual mean precipitation at the Equator; the maximum equatorial insolation: Blue line is the daily insolation in March, greed line is the daily insolation in September, and the red dashed line the maximum of them[59]; the half-precession signal of the equatorial annual mean precipitation

起到了一定的抑制作用, 当斜率的振幅变化越大, 半岁差信号越弱; 当斜率的振幅变化越小, 半岁差信号越强[73]. 而对于其他地区降水变化是否存在半岁差信号以及它们的驱动机制是怎样的; 斜率、岁差、CO_2和冰盖对这些半岁差信号产生了怎样的影响, 这些重要的科学问题都亟需大量长时间尺度的高分辨率降水记录和瞬变模拟实验来探讨.

2.3 轨道驱动在间冰期末期引起的降水突变

气候突变事件和千年尺度气候变化是当前地球科学领域研究的又一重要科学问题, 对现代和未来的全球气候变化具有重要的指示意义. 大量的地质证据表明, 在晚更新世间冰期即将结束的时候会发生气候的突然变冷, 并伴随着一系列的千年尺度气候变化事件[91~95]. 例如, 末次间冰期末期, 格陵兰冰芯和北大西洋沉积物显示, 北半球高纬地区突然显著降温, 并伴随着冰筏碎屑活动的增加和北大西洋深层水形成的减弱[92,95,96]. 与此同时, 石笋和孢粉等记录显示, 欧洲大陆极地林线迅速向南扩张[97]、阿尔卑斯南部突然变冷[98]、地中海沿岸显著变干[99]、东亚夏季风突然减弱[100,101]. 此外, 其他间冰期末期, 石笋等记录也证实了这种突变事件的发生: 奥地利东部石笋记录表明MIS-7e末期欧洲气温显著降低[102]; 中国中部落水洞石笋记录指示MIS-9e末期当地植被状况突然恶化[103], 西南永兴洞石笋记录表明MIS-11c末期东亚夏季风显著减弱[91]. 但目前学术界对这种温暖时期气候突变事件的

驱动机制还不是很清楚.

最近, 利用中等复杂程度的地球系统模型LOVE-CLIM1.3对过去80万年以来11个间冰期的气候开展了不加速的瞬变模拟实验, 对间冰期末期气候突变事件的驱动机制研究取得了新的进展[23]. 研究结果发现, 在间冰期末期, 缓慢变化的太阳辐射可以引起全球范围内快速的气候突变事件. 具体表现为, 当北半球夏季太阳辐射降低到一定阈值时, 会引起大西洋经向翻转环流(Atlantic meridional overturning circulation, AMOC)的突然减弱, 随后发生大幅度的振荡[23]. 间冰期末期AMOC的突然变化主要受控于太阳辐射影响的北极海冰反馈作用, 而温室气体的作用相对较小. 随着太阳辐射的逐渐降低, 北极海冰范围逐渐扩张. 当太阳辐射降低到一定阈值时, 海冰开始覆盖拉布拉多海的对流中心, 导致其对流突然关闭, 引起AMOC的突然减弱. 同时在北欧海北部, 海冰与海洋内部温度的相互作用使得那里的对流产生了百年尺度的高振幅振荡, 从而引起了AMOC的大幅度振荡. 只有当太阳辐射重新升高到一定程度, 使得拉布拉多海和北欧海北部不再被海冰覆盖, 这种AMOC的大幅振荡才会停止.

AMOC的这种变化会引起北半球大范围快速降温事件和全球气候的突变, 总体而言, 北半球气候变化的幅度相对较大, 而南半球气候变化的幅度相对较小[23]. 此外, 模拟的AMOC突变时间与地质记录显示的气候突变时间在测年误差范围内能够很好地对应. 具体而言, MIS-5时期, AMOC突变时间为119.8 ka, 伊比利亚边缘海浮游有孔虫δ^{18}O突变时间为122.4 ka, 格陵兰冰芯δ^{18}O突变时间为119 ka[96], 北大西洋冰筏碎屑沉积物突然增加时间为118 ka[92,95], 董哥洞石笋δ^{18}O突变时间为119.8 ka[100], 三宝洞石笋δ^{18}O突变时间为120.4 ka[101]. MIS-7时期, AMOC突变时间为237.4 ka, 伊比利亚边缘海浮游有孔虫δ^{18}O突变时间为235.8 ka, 奥地利东部石笋δ^{13}C突变时间为239.1 ka[102]. MIS-9时期, AMOC突变时间为323.6 ka, 伊比利亚边缘海浮游有孔虫δ^{18}O突变时间为318.9 ka, 落水洞石笋δ^{18}O突变时间为328.5 ka[103]. MIS-11时期, AMOC突变时间为398.7 ka, 伊比利亚边缘海浮游有孔虫δ^{18}O突变时间为399.5 ka, 永兴洞石笋δ^{18}O突变时间为397.4 ka[91]. 在其他更早的间冰期, AMOC突变时间跟伊比利亚边缘海浮游有孔虫δ^{18}O突变时间均能较好地对应.

就降水而言, 当北半球夏季太阳辐射降低到一定阈值时, 伴随着AMOC的突然减弱和北半球的大范围降温, 不同纬度带的降水也突然减弱, 之后会发生大振幅的振荡(图4). 当降水发生突变后, 其振幅变化能达到之前正常时期的两倍之多, 其变化周期主要为300~600年. 此外, 太阳辐射引起的快速降温事件在北半球高纬度地区短时间内可以形成大量的积雪, 有可能是造成间冰期温暖气候结束、寒冷冰期开始的一个重要因素. 由于不同间冰期太阳辐射的纬度和季节性分布不同, 太阳辐射的临界值在不同间冰期也会略有不同, 但都足够低, 且变化范围较小, 在352.1 W/m^2(MIS-15e)到358.2 W/m^2(MIS-7a)之间. 与过去80万年的间冰期相比, 我们目前所处的间冰期非常特别, 在很长的一段时间内太阳辐射都太高, 不足以达到临界值, 临界值只出现在5万年后, 这与之前通过冰盖模拟得出我们目前所处的间冰期超长、下一个冰期在5万年后才可能出现的结论是一致的[104,105].

3 轨道驱动和冰量对季风降水的相对影响

全球季风作为独特的气候系统, 控制着全球70%人口的生活环境, 深刻影响着人类生存与社会发展[7,9]. 东亚季风作为全球季风系统的重要组成部分[8,108], 其形成、演化及驱动机制长期以来受到广泛关注. 东亚季风多时间尺度(年际-年代际-千年-轨道-构造等尺度)变化对社会生产生活、文明演替乃至人类演化都产生了重要影响[109,110]. 黄土多指标记录表明, 至少在2200万年前现代东亚季风环流格局就已形成[111]. 晚中新世和第四纪以来, 随着青藏高原的阶段性隆升, 东亚季风也存在阶段性增强[12,112,113].

轨道尺度上, 东亚季风变化不仅受到冰期-间冰期旋回的调控[114], 而且在很大程度上受到低纬夏季太阳辐射的影响[77]. 早期理论认为, 轨道尺度的东亚季风变化主要受控于低纬夏季日照量, 且季风快速响应日照量变化, 二者之间仅存在极小的相位差, 即“零相位”假说[115]. 这一观点也得到一些证据的支持, 例如, 季风变化受热带辐合带(inter-tropical convergence zone, ITCZ)季节性摆动的影响, 而ITCZ主要受控于两半球夏季太阳辐射[7,9]. 另外, 石笋记录显示出强烈的2万年岁差周期[77,100,101,116,117]. 然而, 其他的东亚季风地质记录却显示, 东亚季风变化也包含明显的4万年和10万年周期[114,118~121]. 这说明除低纬夏季日照量外, 其他因素(如冰盖)对东亚季风的变化也发挥着重要作用. 因此, 轨道尺度上东亚季风变化的驱动机制还存在着争议, 或许是不同东亚季风记录反映了东亚季风的不同方

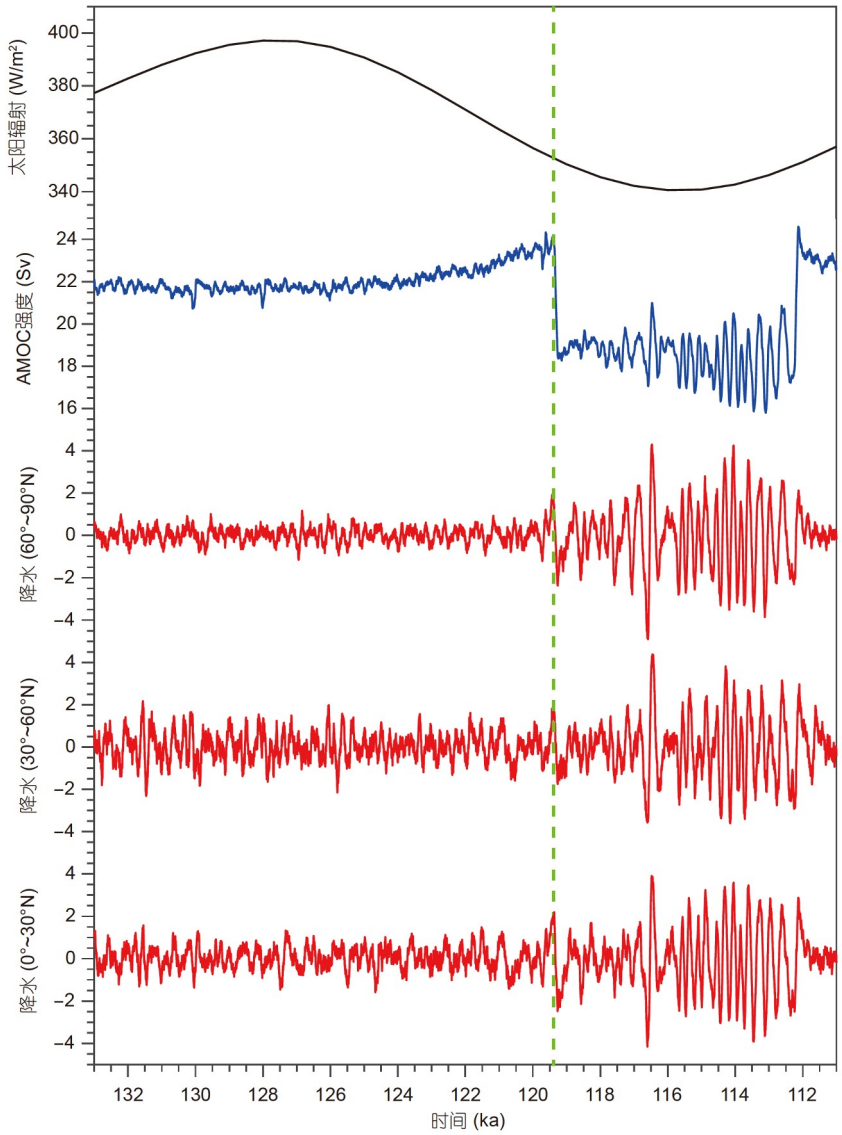

图 4 LOVECLIM模拟的太阳辐射驱动的AMOC和降水变化[23]. 从上到下依次为: 北半球高纬(55°、65°、75°和85°N平均)夏季平均太阳辐射[59,106,107]; AMOC强度[23]; 北半球高纬(60°~90°N)高频降水变化; 北半球中纬(30°~60°N)高频降水变化; 北半球低纬(0°~30°N)高频降水变化. 为了显示不同纬度带降水的高频变化, 对降水序列进行了20%的去趋势处理

Figure 4 LOVECLIM-simulated insolation-only induced variations in AMOC and precipitation[23]. From top to bottom: Mean summer insolation averaged over the four latitudes 55°, 65°, 75°, and 85°N[59,106,107]; AMOC intensity[23]; high-frequency precipitation variation in the Northern Hemisphere (NH) high latitudes (60°–90°N), mid latitudes (30°–60°N) and low latitudes (0°–30°N). In order to show the high-frequency variations of precipitation in different latitudes, the precipitation time series were detrended by subtracting 20% weighted averages

面[122].

除地质记录外, 数值模拟对理解轨道尺度上东亚季风降水的演化规律和动力学机制也发挥着重要作用. 古气候模拟比较计划(PMIP)的多模式结果显示, 相比于工业革命前, 中全新世低纬日照量增加, 海陆热力差异增强, 东亚夏季风增强, 东亚季风区降水面积增大、降水量增加[123]. 而末次冰盛期, 由于大冰盖的作用, 多模式结果显示东亚夏季风减弱, 华北降水减少[124,125]. 末次间冰期, 由于更高的北半球夏季太阳辐射, 东亚夏季风增强, 雨带北移, 导致华北降水增多、华南降水减少[54]. 而过去65万年的全驱动(太阳辐射、温室气体和冰盖共同驱动)瞬变实验结果显示, 东亚夏季风降水以岁差信号占主导, 这进一步说明东亚夏季风主要受控于北半球低纬夏季太阳辐射[126]. HadCM3的敏感性实

验表明, 格陵兰冰盖的消失和南极冰盖的增大均能增强东亚夏季风降水[29].

此外, 利用LOVECLIM对不同冰盖和太阳辐射组合下东亚夏季风降水的变化进行详细分析发现, 冰盖对东亚夏季风降水的影响过程是非线性的, 而且受到太阳辐射的调制[127]. 当北半球夏季太阳辐射较大时, 无论是大冰盖还是小冰盖, 主要通过地形的影响, 欧亚冰盖都能激发向东南方向传输的欧亚波列, 从而加强东亚夏季降水; 而当北半球夏季太阳辐射较小时, 欧亚冰盖对东亚夏季风的影响具有一个阈值, 当冰盖体积超过阈值时, 冰盖主要通过减少海陆热力差异, 减弱东亚夏季风, 进而减少降水. 此外, 最新研究结果发现, 东亚夏季风降水对太阳辐射和冰盖的响应存在着显著的区域差异性[21]. 就整个东亚季风区而言, 夏季降水以岁差信号占主导. 但中国南方(15°~25°N, 105°~120°E)和中国北方(25°~40°N, 105°~120°E)夏季降水却呈现出明显的差别: 中国北方夏季降水以岁差信号占主导, 主要受控于夏季太阳辐射; 而中国南方夏季降水受冰盖影响相对较大, 呈现出明显的10万年周期(图5)[21]. 上述中国南、北方夏季降水对不同外部驱动的差异性响应也被过去30万年利用通用地球系统模式(Community Earth System Model, CESM)进行的加速瞬变实验结果所证实[128].

那么岁差驱动和冰盖驱动是怎样影响东亚季风降水的? 进一步分析得知, 岁差强迫通过改变北半球夏季太阳辐射和纬向海陆热力差异, 引起大气环流异常, 进而影响中国北方夏季降水. 当岁差引起的北半球夏季太阳辐射增强时, 中高纬海陆热力差异增大, 引起东亚大陆气旋式环流异常, 从而使得东亚的偏南风增强, 中国北方夏季降水增多[128]. 而北半球冰盖一方面可以通过改变南北半球间的热力差异, 引起ITCZ的南北移动, 进而影响中国南方降水; 当北半球冰量增加时, 促使

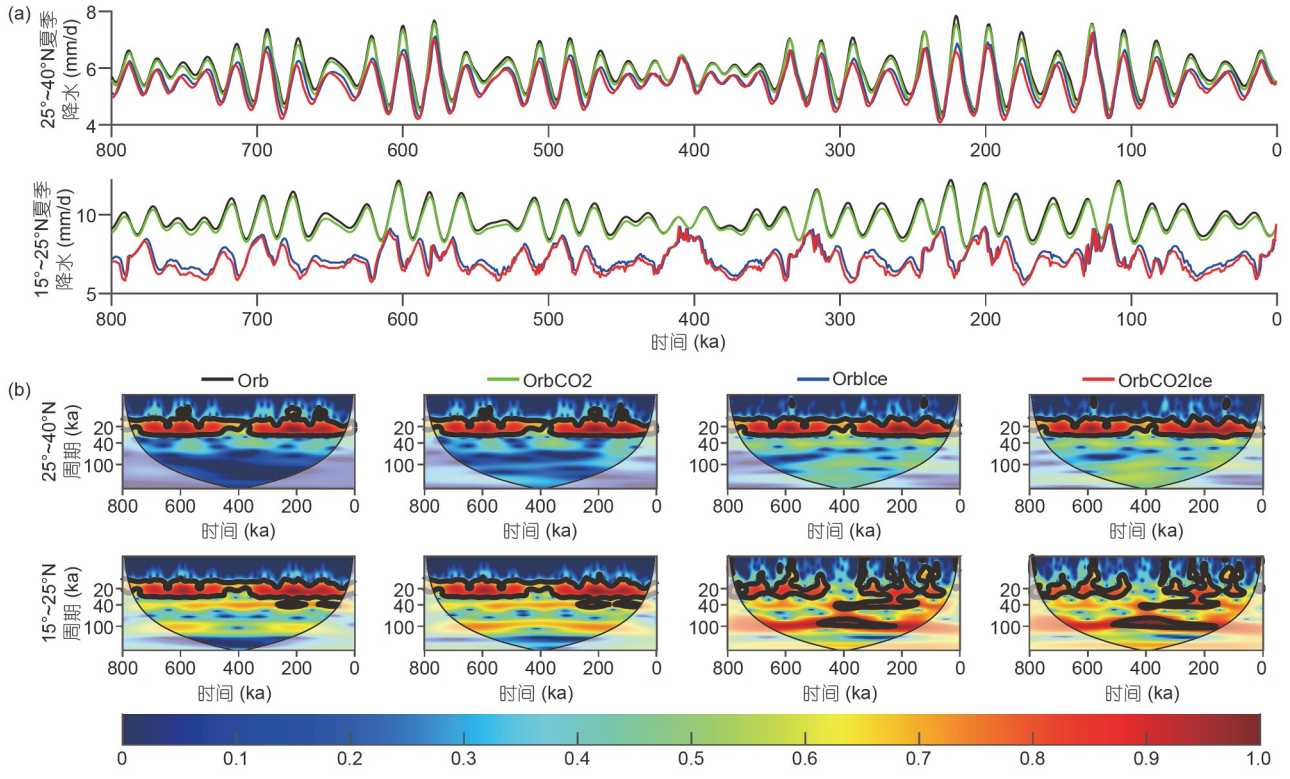

图 5 中国北方和中国南方夏季降水变化及其小波分析结果[21]. (a) HadCM3模拟的中国北方和南方夏季降水[21]. 黑线、绿线、蓝线和红线分别代表了Orb、OrbCO2、OrbIce、OrbCO2Ice的实验结果. (b) 夏季降水的小波分析结果[21]. 第一、二、三、四列分别代表了Orb、OrbCO2、OrbIce、OrbCO2Ice的实验结果

Figure 5 The summer precipitation variations for North China and South China and their wavelet power spectra[21]. (a) HadCM3 emulated summer precipitation for North China and South China[21]. The black, green, blue, and red lines stand for results calculated from Orb, OrbCO2, OrbIce, and OrbCO2Ice, respectively. (b) Wavelet spectrum analysis for summer precipitation[21]. The first, second, third, and fourth column stand for results calculated from Orb, OrbCO2, OrbIce, and OrbCO2Ice, respectively

ITCZ向南移动, 中国南方夏季降水减少[21]. 另一方面, 欧亚大陆冰量增加, 冰盖能在对流层上空激发出反气旋异常, 通过欧亚大陆上空副热带急流中罗斯贝波传递到蒙古-西伯利亚上空并强迫出气旋式异常, 同时在中国南方地区上空也能强迫出反气旋环流异常, 并且向对流层下部传递, 抑制了对流层低层的水汽辐合, 导致中国南方地区夏季降水减少[127,128].

除东亚季风降水外, 太阳辐射和冰盖也显著影响了其他季风区. 中国南方鹤庆古湖钻孔记录重建的印度夏季风显示, 其不仅有明显的偏心率(100 ka)和岁差(23和19 ka)周期, 还存在明显的73、55和29 ka周期, 并认为其受到北半球冰量和南半球潜热释放等共同作用[129]. 而印度洋钻孔记录显示印度夏季风降水也含有岁差周期, 但其滞后于夏季太阳辐射约9 ka, 且岁差信号仅占印度夏季风降水周期信号的30%, 研究认为印度季风和东亚季风降水具有不同的外部驱动力[130]. 相比之下, 其他季风区降水变化与轨道驱动相关的研究相对较少. 地中海沉积物指示的非洲夏季风变化具有明显的岁差和斜率信号, 且以岁差信号占主导. 当岁差较少时, 非洲夏季风增强并向北扩展[131,132]. 亚马逊盆地钻孔含铁磁性矿物的比值重建的南美季风降水变化显示, 南美季风降水变化要领先于冰盖变化, 这说明热带季风降水变化是调控冰盖变化的驱动因子, 而不是单纯地响应于冰盖变化, 该地区季风降水变化受控于两半球夏季太阳辐射共同调控的热带辐合带的季节性摆动[133]. 为了更好地探讨全球季风降水变化对不同外部驱动力的响应, 未来研究中不仅需要获取更多长时间尺度、高分辨率且季风降水意义明确的地质记录, 同时也需要加强不同模型瞬变模拟研究.

4 结论与展望

本文通过对水循环的两个重要组成部分(海冰和降水)轨道尺度变化的最近研究进行了总结和归纳, 重点强调了海冰与降水对岁差、斜率、CO_2和冰盖的区域差异性响应, 得到了以下几点初步结论.

(1) 轨道尺度上, 北半球海冰主要受控于太阳辐射和岁差, 而南半球海冰主要受控于CO_2和斜率. 南北半球海冰的区域差异性响应, 其根本原因主要是北冰洋和南大洋所处地理位置的不同及其南北半球海陆分布的不同.

(2) 对全球降水而言, 不同区域降水对岁差、斜率和CO_2的响应随地区和时间而变化. 相对于太阳辐射, CO_2对轨道尺度上全球降水的影响相对较弱.

(3) 热带地区降水变化不仅有非常强烈的岁差信号, 而且还有很明显的半岁差信号, 其半岁差信号主要是响应赤道最大太阳辐射.

(4) 间冰期末期, 当太阳辐射降低到一定阈值时, 会引起AMOC的突然减弱, 进而引起全球气候突变. 同时, 不同纬度带的降水也会发生大振幅的振荡.

(5) 中国南方夏季降水受冰盖影响显著, 冰盖主要通过影响ITCZ的摆动来影响降水, 而中国北方夏季降水以岁差信号为主, 主要受太阳辐射控制. 此外, 冰盖对东亚夏季风的影响具有很强的区域性和非线性特征, 与太阳辐射的高低以及冰盖的大小、位置、形状均有关.

在未来的研究中, 为了更好地理解轨道尺度上海冰和降水的变化, 以下几个方面需要提高: 首先, 在地质记录方面, 需要获得更多不同地区具有精确定年、高分辨率且古气候指示意义明确的海冰和降水记录; 辨析记录的季节性, 加强海冰和降水的季节重建. 其次, 在古气候模拟方面, 需要通过耦合冰盖发育模块和改进植被动态模型等提高气候模型对轨道尺度降水和海冰的模拟能力; 进一步完善同位素耦合的地球系统模型, 实现模拟结果与古气候记录直接对比. 最后, 地质记录重建与气候模式模拟的结合和数据同化, 将会是未来地球系统科学领域发展的长期趋势和重要方向, 这一方面的合作研究亟须加强. 只有更全面地理解海冰和降水轨道尺度的变化, 才能更好地探讨轨道尺度的全球水循环, 进而为提高对水循环地质演变的认识作出重要贡献.

参考文献

1 Bowen G J, Cai Z, Fiorella R P, et al. Isotopes in the water cycle: Regional- to global-scale patterns and applications. Annu Rev Earth Planet Sci, 2019, 47: 453–479

2 Huang E, Wang P, Wang Y, et al. Dole effect as a measurement of the low-latitude hydrological cycle over the past 800 ka. Sci Adv, 2020, 6: eaba4823

3 Guo Z, Zhou X, Wu H. Glacial-interglacial water cycle, global monsoon and atmospheric methane changes. Clim Dyn, 2012, 39: 1073–1092

4 Wang P X, Li Q Y, Tian J, et al. Long-term cycles in the carbon reservoir of the Quaternary ocean: A perspective from the South China Sea. Natl Sci Rev, 2014, 1: 119–143
5 Raymo M E, Lisiecki L E, Nisancioglu K H. Plio-Pleistocene ice volume, Antarctic climate, and the global δ^{18}O record. Science, 2006, 313: 492–495
6 Wang P, Wang B, Kiefer T. Global Monsoon across timescales. Clim Dyn, 2012, 39: 1043–1044
7 Wang P X, Wang B, Cheng H, et al. The global monsoon across timescales: Coherent variability of regional monsoons. Clim Past, 2014, 10: 2007–2052
8 An Z S, Wu G X, Li J P, et al. Global monsoon dynamics and climate change. Annu Rev Earth Planet Sci, 2015, 43: 29–77
9 Wang P X, Wang B, Cheng H, et al. The global monsoon across time scales: Mechanisms and outstanding issues. Earth-Sci Rev, 2017, 174: 84–121
10 Westerhold T, Marwan N, Drury A J, et al. An astronomically dated record of Earth's climate and its predictability over the last 66 million years. Science, 2020, 369: 1383–1387
11 Hays J D, Imbrie J, Shackleton N J. Variations in the Earth's orbit: Pacemaker of the ice ages. Science, 1976, 194: 1121–1132
12 Guo Z T, Berger A, Yin Q Z, et al. Strong asymmetry of hemispheric climates during MIS-13 inferred from correlating China loess and Antarctica ice records. Clim Past, 2009, 5: 21–31
13 Hao Q, Wang L, Oldfield F, et al. Delayed build-up of Arctic ice sheets during 400000-year minima in insolation variability. Nature, 2012, 490: 393–396
14 Hao Q Z, Wang L, Oldfield F, et al. Extra-long interglacial in Northern Hemisphere during MISs 15-13 arising from limited extent of Arctic ice sheets in glacial MIS 14. Sci Rep, 2015, 5: 12103
15 Wolff E W, Fischer H, Fundel F, et al. Southern Ocean sea-ice extent, productivity and iron flux over the past eight glacial cycles. Nature, 2006, 440: 491–496
16 Sun Y B, Yin Q Z, Crucifix M, et al. Diverse manifestations of the mid-Pleistocene climate transition. Nat Commun, 2019, 10: 352
17 Li M S, Huang C J, Hinnov L, et al. Obliquity-forced climate during the Early Triassic hothouse in China. Geology, 2016, 44: 623–626
18 Li M S, Hinnov L A, Huang C J, et al. Sedimentary noise and sea levels linked to land-ocean water exchange and obliquity forcing. Nat Commun, 2018, 9: 1004
19 Wu Z, Yin Q, Guo Z, et al. Hemisphere differences in response of sea surface temperature and sea ice to precession and obliquity. Glob Planet Change, 2020, 192: 103223
20 Wu Z, Yin Q, Guo Z, et al. Comparison of Arctic and Southern Ocean sea ice between the last nine interglacials and the future. Clim Dyn, 2022, 59: 519–529
21 Lyu A Q, Yin Q Z, Crucifix M, et al. Diverse regional sensitivity of summer precipitation in East Asia to ice volume, CO_2 and astronomical forcing. Geophys Res Lett, 2021, 48: e2020GL092005
22 Lu H, Yin Q Z, Wu Z P, et al. Insolation and CO_2 impacts on the spatial differences of the MIS-9 and MIS-11 climate between monsoonal China and central Asia. J Geophys Res Atmos, 2022, 127: e2022JD036505
23 Yin Q Z, Wu Z P, Berger A, et al. Insolation triggered abrupt weakening of Atlantic circulation at the end of interglacials. Science, 2021, 373: 1035–1040
24 Wagreich M, Lein R, Sames B. Eustasy, its controlling factors, and the limno-eustatic hypothesis-concepts inspired by Eduard Suess. Austrian J Earth Sci, 2014, 107: 115–131
25 Sames B, Wagreich M, Conrad C P, et al. Aquifer-eustasy as the main driver of short-term sea-level fluctuations during Cretaceous hothouse climate phases. Geol Soc Lond Spec Publ, 2020, 498: 9–38
26 Wang M, Chen H, Huang C, et al. Astronomical forcing and sedimentary noise modeling of lake-level changes in the Paleogene Dongpu Depression of North China. Earth Planet Sci Lett, 2020, 535: 116116
27 Wang M, Li M, Kemp D B, et al. Sedimentary noise modeling of lake-level change in the Late Triassic Newark Basin of North America. Glob Planet Change, 2022, 208: 103706
28 Serreze M C, Barry R G. Processes and impacts of Arctic amplification: A research synthesis. Glob Planet Change, 2011, 77: 85–96
29 Shi F, Yin Q, Nikolova I, et al. Impacts of extremely asymmetrical polar ice sheets on the East Asian summer monsoon during the MIS-13 interglacial. Quat Sci Rev, 2020, 230: 106164
30 Sun Y, Wang T, Yin Q, et al. A review of orbital-scale monsoon variability and dynamics in East Asia during the Quaternary. Quat Sci Rev, 2022, 288: 107593
31 Goosse H, Roche D M, Mairesse A, et al. Modelling past sea ice changes. Quat Sci Rev, 2013, 79: 191–206
32 Hobbs W R, Massom R, Stammerjohn S, et al. A review of recent changes in Southern Ocean sea ice, their drivers and forcings. Glob Planet Change, 2016, 143: 228–250

33 Krinner G, Magand O, Simmonds I, et al. Simulated Antarctic precipitation and surface mass balance at the end of the twentieth and twenty-first centuries. Clim Dyn, 2007, 28: 215–230

34 Delille B, Vancoppenolle M, Geilfus N X, et al. Southern Ocean CO_2 sink: The contribution of the sea ice. J Geophys Res Oceans, 2014, 119: 6340–6355

35 Hillaire-Marcel C, de Vernal A. Stable isotope clue to episodic sea ice formation in the glacial North Atlantic. Earth Planet Sci Lett, 2008, 268: 143–150

36 Wollenburg J E, Knies J, Mackensen A. High-resolution paleoproductivity fluctuations during the past 24 kyr as indicated by benthic foraminifera in the marginal Arctic Ocean. Palaeogeogr Palaeoclimatol Palaeoecol, 2004, 204: 209–238

37 Scott D B, Schell T, St-Onge G, et al. Foraminiferal assemblage changes over the last 15000 years on the Mackenzie-Beaufort Sea Slope and Amundsen Gulf, Canada: Implications for past sea ice conditions. Paleoceanography, 2009, 24: PA2219

38 de Vernal A, Hillaire-Marcel C, Darby D A. Variability of sea ice cover in the Chukchi Sea (western Arctic Ocean) during the Holocene. Paleoceanography, 2005, 20: PA4018

39 Backman J, Fornaciari E, Rio D. Biochronology and paleoceanography of late Pleistocene and Holocene calcareous nannofossil abundances across the Arctic Basin. Mar Micropaleontol, 2009, 72: 86–98

40 Darby D A, Ortiz J, Polyak L, et al. The role of currents and sea ice in both slowly deposited central Arctic and rapidly deposited Chukchi-Alaskan margin sediments. Glob Planet Change, 2009, 68: 58–72

41 Andrews J T, Darby D, Eberle D, et al. A robust, multisite Holocene history of drift ice off northern Iceland: Implications for North Atlantic climate. Holocene, 2009, 19: 71–77

42 Bennike O. Holocene sea-ice variations in Greenland: Onshore evidence. Holocene, 2004, 14: 607–613

43 Vare L L, Massé G, Gregory T R, et al. Sea ice variations in the central Canadian Arctic Archipelago during the Holocene. Quat Sci Rev, 2009, 28: 1354–1366

44 Lo L, Belt S T, Lattaud J, et al. Precession and atmospheric CO_2 modulated variability of sea ice in the central Okhotsk Sea since 130000 years ago. Earth Planet Sci Lett, 2018, 488: 36–45

45 Stein R, Fahl K, Gierz P, et al. Arctic Ocean sea ice cover during the penultimate glacial and the last interglacial. Nat Commun, 2017, 8: 373

46 Cronin T M, Gemery L, Briggs W M J, et al. Quaternary Sea-ice history in the Arctic Ocean based on a new Ostracode sea-ice proxy. Quat Sci Rev, 2010, 29: 3415–3429

47 Cronin T M, Polyak L, Reed D, et al. A 600-ka Arctic sea-ice record from Mendeleev Ridge based on ostracodes. Quat Sci Rev, 2013, 79: 157–167

48 Cronin T M, Dwyer G S, Caverly E K, et al. Enhanced Arctic amplification began at the Mid-Brunhes Event ~400000 years ago. Sci Rev, 2017, 7: 14475

49 Berger M, Brandefelt J, Nilsson J. The sensitivity of the Arctic sea ice to orbitally induced insolation changes: A study of the mid-Holocene Paleoclimate Modelling Intercomparison Project 2 and 3 simulations. Clim Past, 2013, 9: 969–982

50 Renssen H, Goosse H, Fichefet T, et al. Holocene climate evolution in the high-latitude Southern Hemisphere simulated by a coupled atmosphere-sea ice-ocean-vegetation model. Holocene, 2005, 15: 951–964

51 Roche D M, Crosta X, Renssen H. Evaluating Southern Ocean sea-ice for the Last Glacial Maximum and pre-industrial climates: PMIP-2 models and data evidence. Quat Sci Rev, 2012, 56: 99–106

52 Guarino M V, Sime L C, Schröeder D, et al. Sea-ice-free Arctic during the Last Interglacial supports fast future loss. Nat Clim Chang, 2020, 10: 928–932

53 Otto-Bliesner B L, Brady E C, Tomas R A, et al. A comparison of the CMIP6 midHolocene and lig127k simulations in CESM2. Paleoceanogr Paleoclimatol, 2020, 35: e2020PA003957

54 Otto-Bliesner B L, Brady E C, Zhao A, et al. Large-scale features of Last Interglacial climate: Results from evaluating the lig127k simulations for the Coupled Model Intercomparison Project (CMIP6)-Paleoclimate Modeling Intercomparison Project (PMIP4). Clim Past, 2021, 17: 63–94

55 Kageyama M, Sime L C, Sicard M, et al. A multi-model CMIP6-PMIP4 study of Arctic sea ice at 127 ka: Sea ice data compilation and model differences. Clim Past, 2021, 17: 37–62

56 Timmermann A, Friedrich T, Timm O E, et al. Modeling obliquity and CO_2 effects on Southern Hemisphere climate during the past 408 ka. J Clim, 2014, 27: 1863–1875

57 Yin Q Z, Berger A. Individual contribution of insolation and CO_2 to the interglacial climates of the past 800000 years. Clim Dyn, 2012, 38: 709–724

58 Berger A, Loutre M F, Yin Q. Total irradiation during any time interval of the year using elliptic integrals. Quat Sci Rev, 2010, 29: 1968–1982

59 Berger A L. Long-term variations of caloric insolation resulting from the Earth's orbital elements. Quat Res, 1978, 9: 139–167

60 Yin Q, Berger A. Interglacial analogues of the Holocene and its natural near future. Quat Sci Rev, 2015, 120: 28–46

61 Moseley G E, Edwards R L, Lord N S, et al. Speleothem record of mild and wet mid-Pleistocene climate in northeast Greenland. Sci Adv, 2021, 7: eabe1260
62 Tarasov P, Bezrukova E, Karabanov E, et al. Vegetation and climate dynamics during the Holocene and Eemian interglacials derived from Lake Baikal pollen records. Palaeogeogr Palaeoclimatol Palaeoecol, 2007, 252: 440–457
63 Routson C C, McKay N P, Kaufman D S, et al. Mid-latitude net precipitation decreased with Arctic warming during the Holocene. Nature, 2019, 568: 83–87
64 Deininger M, McDermott F, Cruz F W, et al. Inter-hemispheric synchroneity of Holocene precipitation anomalies controlled by Earth's latitudinal insolation gradients. Nat Commun, 2020, 11: 5447
65 Hayashi R, Sagawa T, Irino T, et al. Orbital-scale vegetation-ocean-atmosphere linkages in western Japan during the last 550 ka based on a pollen record from the IODP site U1427 in the Japan Sea. Quat Sci Rev, 2021, 267: 107103
66 Baker P A, Seltzer G O, Fritz S C, et al. The history of South American tropical precipitation for the past 25000 years. Science, 2001, 291: 640–643
67 Hou A, Bahr A, Chiessi C M, et al. Obliquity influence on low-latitude coastal precipitation in eastern Brazil during the past ~850 kyr. Paleoceanogr Paleoclimatol, 2022, 37: e2021PA004238
68 Oliveira D, Desprat S, Yin Q, et al. Unraveling the forcings controlling the vegetation and climate of the best orbital analogues for the present interglacial in SW Europe. Clim Dyn, 2018, 51: 667–686
69 Martínez-Dios A, Pelejero C, Cobacho S, et al. A 1-million-year record of environmental change in the central Mediterranean Sea from organic molecular proxies. Paleoceanogr Paleoclimatol, 2021, 36: e2021PA004289
70 Wagner B, Vogel H, Francke A, et al. Mediterranean winter rainfall in phase with African monsoons during the past 1.36 million years. Nature, 2019, 573: 256–260
71 Donders T, Panagiotopoulos K, Koutsodendris A, et al. 1.36 million years of Mediterranean forest refugium dynamics in response to glacial-interglacial cycle strength. Proc Natl Acad Sci USA, 2021, 118: e2026111118
72 Evans G, Augustinus P, Gadd P, et al. Millennial-scale periodicities associated with changes in wind ansd precipitation over the last Glacial cycle (ca. 117 ± 8.5 ka BP) recorded in sediments from Lake Kai Iwi, Northland, New Zealand. Glob Planet Change, 2022, 208: 103688
73 Su Q Q, Lyu A Q, Wu Z P, et al. Diverse response of global terrestrial vegetation to astronomical forcing and CO_2 during the MIS-11 and MIS-13 interglacials. Clim Dyn, 2022, doi: doi.org/10.1007/s00382-022-06308-y
74 Shin S I, Sardeshmukh P D, Webb R S, et al. Understanding the mid-Holocene climate. J Clim, 2006, 19: 2801–2817
75 Harrison S P, Kutzbach J E, Liu Z, et al. Mid-Holocene climates of the Americas: A dynamical response to changed seasonality. Clim Dyn, 2003, 20: 663–688
76 Williams J W, Shuman B, Bartlein P J, et al. Rapid, time-transgressive, and variable responses to early Holocene midcontinental drying in North America. Geology, 2010, 38: 135–138
77 Cheng H, Edwards R L, Sinha A, et al. The Asian monsoon over the past 640000 years and ice age terminations. Nature, 2016, 534: 640–646
78 Kathayat G, Cheng H, Sinha A, et al. Indian monsoon variability on millennial-orbital timescales. Sci Rep, 2016, 6: 1–7
79 Berger A, Loutre M F, Mélice J L. Equatorial insolation: From precession harmonics to eccentricity frequencies. Clim Past, 2006, 2: 131–136
80 Hinnov L A, Schulz M, Yiou P. Interhemispheric space-time attributes of the Dansgaard-Oeschger oscillations between 100 and 0 ka. Quat Sci Rev, 2002, 21: 1213–1228
81 Rutherford S, D'Hondt S. Early onset and tropical forcing of 100000-year Pleistocene glacial cycles. Nature, 2000, 408: 72–75
82 Ferretti P, Crowhurst S J, Hall M A, et al. North Atlantic millennial-scale climate variability 910 to 790 ka and the role of the equatorial insolation forcing. Earth Planet Sci Lett, 2010, 293: 28–41
83 Ferretti P, Crowhurst S J, Naafs B D A, et al. The Marine Isotope Stage 19 in the mid-latitude North Atlantic Ocean: Astronomical signature and intra-interglacial variability. Quat Sci Rev, 2015, 108: 95–110
84 Turney C S M, Kershaw A P, Clemens S C, et al. Millennial and orbital variations of El Niño/Southern Oscillation and high-latitude climate in the last glacial period. Nature, 2004, 428: 306–310
85 Trauth M H, Deino A L, Bergner A G N, et al. East African climate change and orbital forcing during the last 175 kyr BP. Earth Planet Sci Lett, 2003, 206: 297–313
86 Sun J, Huang X. Half-precessional cycles recorded in Chinese loess: Response to low-latitude insolation forcing during the Last Interglaciation. Quat Sci Rev, 2006, 25: 1065–1072
87 Olago D. Long-term temporal characteristics of palaeomonsoon dynamics in equatorial Africa. Glob Planet Change, 2000, 26: 159–171
88 Thevenon F, Bard E, Williamson D, et al. A biomass burning record from the West Equatorial Pacific over the last 360 ky: Methodological, climatic and anthropic implications. Palaeogeogr Palaeoclimatol Palaeoecol, 2004, 213: 83–99
89 Trauth M H, Asrat A, Cohen A S, et al. Recurring types of variability and transitions in the ~620 kyr record of climate change from the Chew

Bahir basin, southern Ethiopia. Quat Sci Rev, 2021, 266: 106777
90 Tuenter E, Weber S L, Hilgen F J, et al. Simulating sub-Milankovitch climate variations associated with vegetation dynamics. Clim Past, 2007, 3: 169–180
91 Zhao X, Cheng H, Sinha A, et al. A high-resolution speleothem record of Marine Isotope Stage 11 as a natural analog to Holocene Asian summer monsoon variations. Geophys Res Lett, 2019, 46: 9949–9957
92 Oppo D W, McManus J F, Cullen J L. Evolution and demise of the Last Interglacial warmth in the subpolar North Atlantic. Quat Sci Rev, 2006, 25: 3268–3277
93 Mokeddem Z, McManus J F, Oppo D W. Oceanographic dynamics and the end of the last interglacial in the subpolar North Atlantic. Proc Natl Acad Sci USA, 2014, 111: 11263–11268
94 Irvalı N, Galaasen E V, Ninnemann U S, et al. A low climate threshold for south Greenland Ice Sheet demise during the Late Pleistocene. Proc Natl Acad Sci USA, 2020, 117: 190–195
95 Galaasen E V, Ninnemann U S, Irvalı N, et al. Rapid reductions in North Atlantic Deep Water during the peak of the last interglacial period. Science, 2014, 343: 1129–1132
96 North Greenland Ice Core Project Members. High-resolution record of Northern Hemisphere climate extending into the last interglacial period. Nature, 2004, 431: 147–151
97 Müller U C, Kukla G J. North Atlantic Current and European environments during the declining stage of the last interglacial. Geology, 2004, 32: 1009–1012
98 Meyer M C, Spötl C, Mangini A. The demise of the Last Interglacial recorded in isotopically dated speleothems from the Alps. Quat Sci Rev, 2008, 27: 476–496
99 Bar-Matthews M, Ayalon A, Gilmour M, et al. Sea-land oxygen isotopic relationships from planktonic foraminifera and speleothems in the Eastern Mediterranean region and their implication for paleorainfall during interglacial intervals. Geochim Cosmochim Acta, 2003, 67: 3181–3199
100 Yuan D, Cheng H, Edwards R L, et al. Timing, duration, and transitions of the last interglacial Asian monsoon. Science, 2004, 304: 575–578
101 Wang Y, Cheng H, Edwards R L, et al. Millennial- and orbital-scale changes in the East Asian monsoon over the past 224000 years. Nature, 2008, 451: 1090–1093
102 Spotl C, Scholz D, Mangini A. A terrestrial U/Th-dated stable isotope record of the Penultimate Interglacial. Earth Planet Sci Lett, 2008, 276: 283–292
103 Yang S, Chen S, Wang Y, et al. Millennial-scale Asian monsoon variability during MIS 9 revealed by a high-resolution stalagmite $\delta^{18}O$ record in Luoshui Cave, central China. Quat Sci Rev, 2020, 234: 106218
104 Berger A, Loutre M F. An exceptionally long interglacial ahead? Science, 2002, 297: 1287–1288
105 Ganopolski A, Winkelmann R, Schellnhuber H J. Critical insolation-CO_2 relation for diagnosing past and future glacial inception. Nature, 2016, 529: 200–203
106 Berger A, Loutre M F. Insolation values for the climate of the last 10 million years. Quat Sci Rev, 1991, 10: 297–317
107 Berger A, Yin Q Z. Astronomical theory and orbital forcing. In: Matthews J A, ed. The SAGE Handbook of Environmental Change. London: SAGE Publications Ltd., 2012, 1: 405–425
108 Cheng H, Sinha A, Wang X, et al. The Global Paleomonsoon as seen through speleothem records from Asia and the Americas. Clim Dyn, 2012, 39: 1045–1062
109 Zhang P, Cheng H, Edwards R L, et al. A test of climate, sun, and culture relationships from an 1810-year Chinese cave record. Science, 2008, 322: 940–942
110 Zhang H, Cheng H, Sinha A, et al. Collapse of the Liangzhu and other Neolithic cultures in the lower Yangtze region in response to climate change. Sci Adv, 2021, 7: eabi9275
111 Guo Z T, Ruddiman W F, Hao Q Z, et al. Onset of Asian desertification by 22 Myr ago inferred from loess deposits in China. Nature, 2002, 416: 159–163
112 Ding Z L, Xiong S F, Sun J M, et al. Pedostratigraphy and paleomagnetism of a ~7.0 Ma eolian loess-red clay sequence at Lingtai, Loess Plateau, north-central China and the implications for paleomonsoon evolution. Palaeogeogr Palaeoclimatol Palaeoecol, 1999, 152: 49–66
113 Ding Z L, Yang S L, Sun J M, et al. Iron geochemistry of loess and red clay deposits in the Chinese Loess Plateau and implications for long-term Asian monsoon evolution in the last 7.0 Ma. Earth Planet Sci Lett, 2001, 185: 99–109
114 Guo Z, Biscaye P, Wei L, et al. Summer monsoon variations over the last 1.2 Ma from the weathering of loess-soil sequences in China. Geophys Res Lett, 2000, 27: 1751–1754
115 Kutzbach J E. Monsoon climate of the Early Holocene: Climate experiment with the Earth's orbital parameters for 9000 years ago. Science, 1981, 214: 59–61

116 Cheng H, Edwards R L, Broecker W S, et al. Ice age terminations. Science, 2009, 326: 248–252
117 Cheng H, Zhang H, Zhao J, et al. Chinese stalagmite paleoclimate researches: A review and perspective. Sci China Earth Sci, 2019, 62: 1489–1513
118 Tian J, Wang P, Cheng X. Development of the East Asian monsoon and Northern Hemisphere glaciation: Oxygen isotope records from the South China Sea. Quat Sci Rev, 2004, 23: 2007–2016
119 Clemens S C, Prell W L, Sun Y, et al. Southern Hemisphere forcing of Pliocene δ^{18}O and the evolution of Indo-Asian monsoons. Paleoceanography, 2008, 23: PA4210
120 Li T, Liu F, Abels H A, et al. Continued obliquity pacing of East Asian summer precipitation after the mid-Pleistocene transition. Earth Planet Sci Lett, 2017, 457: 181–190
121 Zhao Y, Tzedakis P C, Li Q, et al. Evolution of vegetation and climate variability on the Tibetan Plateau over the past 1.74 million years. Sci Adv, 2020, 6: eaay6193
122 Cheng H, Zhang H, Cai Y, et al. Orbital-scale Asian summer monsoon variations: Paradox and exploration. Sci China Earth Sci, 2021, 64: 529–544
123 Jiang D, Lang X, Tian Z, et al. Mid-Holocene East Asian summer monsoon strengthening: Insights from Paleoclimate Modeling Intercomparison Project (PMIP) simulations. Palaeogeogr Palaeoclimatol Palaeoecol, 2013, 369: 422–429
124 Jiang D, Lang X. Last glacial maximum East Asian monsoon: Results of PMIP simulations. J Clim, 2010, 23: 5030–5038
125 Jiang D, Tian Z, Lang X, et al. The concept of global monsoon applied to the last glacial maximum: A multi-model analysis. Quat Sci Rev, 2015, 126: 126–139
126 Weber S L, Tuenter E. The impact of varying ice sheets and greenhouse gases on the intensity and timing of boreal summer monsoons. Quat Sci Rev, 2011, 30: 469–479
127 Yin Q Z, Berger A, Crucifix M. Individual and combined effects of ice sheets and precession on MIS-13 climate. Clim Past, 2009, 5: 229–243
128 Xie X X, Liu X D. Regional differences of East Asian monsoon precipitation in response to orbital forcing and global ice-volume changes since the late Middle Pleistocene (in Chinese). Quat Sci, 2020, 40: 1486–1498 [谢小训, 刘晓东. 晚中更新世以来东亚季风降水变化对轨道强迫和全球冰量变动响应的区域差异. 第四纪研究, 2020, 40: 1486–1498]
129 An Z S, Steven C C, Ji S, et al. Glacial-interglacial Indian summer monsoon dynamics. Science, 2011, 333: 719–723
130 Gebregiorgis D, Hathorne E C, Giosan L, et al. Southern Hemisphere forcing of South Asian monsoon precipitation over the past ~1 million years. Nat Commun, 2018, 9: 4702
131 Lourens L J, Antonarakou A, Hilgen F J, et al. Evaluation of the Plio-Pleistocene astronomical timescale. Paleoceanography, 1996, 11: 391–413
132 Tuenter E, Weber S L, Hilgen F J, et al. The response of the African summer monsoon to remote and local forcing due to precession and obliquity. Glob Planet Change, 2003, 36: 219–235
133 Harris S E, Mix A C. Pleistocene precipitation balance in the Amazon Basin recorded in deep sea sediments. Quat Res, 1999, 51: 14–26

Summary for “轨道驱动对高低纬水循环的影响特征: 海冰和降水”

The effect of astronomical forcing on water cycle: Sea ice and precipitation

Zhipeng Wu[1,2,3], Qiuzhen Yin[2*], Mingqiang Liang[2], Zhengtang Guo[1,3,4], Feng Shi[1,4], Hao Lu[1], Qianqian Su[2] & Anqi Lü[2]

[1] *Key Laboratory of Cenozoic Geology and Environment, Institute of Geology and Geophysics, Chinese Academy of Sciences, Beijing 100029, China;*
[2] *Georges Lemaître Center for Earth and Climate Research, Earth and Life Institute, Université catholique de Louvain, Louvain-la-Neuve 1348, Belgium;*
[3] *College of Earth and Planetary Sciences, University of Chinese Academy of Sciences, Beijing 100049, China;*
[4] *Center for Excellence in Life and Paleoenvironment, Chinese Academy of Sciences, Beijing 100044, China*
* Corresponding author, E-mail: qiuzhen.yin@uclouvain.be

Understanding the variations of water cycle on orbital timescale and their response to astronomical parameters, greenhouse gases (GHG) and ice sheets is one of the focuses in paleoclimate study. Sea ice and precipitation, two important components of the water cycle, are paid much attention. A better understanding of their variations on orbital timescale, especially their response to external forcing and related processes and feedbacks, could provide insight on their long-term variations in the future. The latest research results show that, on orbital scale, the Arctic sea ice is more sensitive to insolation, while the Southern Ocean sea ice is more sensitive to GHG. Under the combined influence of insolation and GHG, the last nine interglacials all have much less summer Arctic sea ice, as compared to both the present-day and the future, due to the much higher Northern Hemisphere (NH) summer insolation. As compared to the future, the last nine interglacials all have much more annual and seasonal Southern Ocean sea ice due to their much lower CO_2. In terms of the astronomical parameters, the Arctic sea ice is more influenced by precession, whereas obliquity plays a more important role in the Southern Ocean sea ice. The different responses of Arctic and Southern Ocean sea ice to astronomical parameters and CO_2 are mainly due to their different geographical locations. The Arctic ocean is relatively closed and it is located in the northern highest latitudes, which make it only receives very little insolation during winter and it is mainly influenced by precession-dominated summer insolation. The summer insolation not only influences the summer Arctic sea ice, but also has an effect on the winter one through the summer remnant effect. In addition, the Arctic sea ice is also affected by the vegetation in the northern mid and high latitudes, which is mainly dominated by precession. As compared to the Arctic, the latitudes of Southern Ocean are lower and it is more open, which make it is more sensitive to the annual insolation and CO_2. The relative effect of precession, obliquity and CO_2 on precipitation largely depends on different regions and time periods. The tropical precipitation changes also show obvious half-precession cycles in response to the maximum equatorial insolation. In addition, astronomically-induced slow variation of insolation can trigger abrupt changes of the Atlantic meridional circulation (AMOC) through sea ice-ocean interactions in the Labrador and Nordic Seas, consequently leading to abrupt oscillations in large-scale temperature and precipitation. In East Asia, the summer precipitation in the northern part is more influenced by insolation, with a dominant precession signal. Precession-dominated insolation can influence the atmospheric circulation through its effect on the land-sea thermal contrast, which finally affects the summer monsoon precipitation. However, the summer precipitation in the southern region is more influenced by ice sheets, by their control on the meridional movement of the Inter-tropical Convergence Zone (ITCZ). In addition, the Eurasian ice sheet can further influence the precipitation in the southern part through a south-eastwards perturbation planetary wave. Moreover, the effects of insolation and ice sheets on the summer monsoon precipitation show strong regional and nonlinear characteristics, which depend on the extent, height and location of the ice sheets and the intensity of insolation.

water cycle, precipitation, sea ice, orbital forcing, ice sheets, high-low latitudes interactions

doi: 10.1360/TB-2022-0833